TPM Vol. 32, No. S6, 2025
ISSN: 1972-6325
https://www.tpmap.org/

ANALYSIS OF AN INVERTED HORSESHOE-SHAPED HYDRAULIC POWER SINK USING AUTODESK CFD AND AN EXPERIMENTAL MODEL

ARAUJO CARMONA MARTIN JOZEF
CIVIL ENGINEERING UNDERGRADUATE STUDENT, UNIVERSIDAD PRIVADA DEL NORTE, FACULTY OF ENGINEERING, LIMA, PERÚ
EMAIL: n00328443@upn.pe, ORCID ID: HTTPS://ORCID.ORG/0009-0000-4546-216X

CALIXTO SALAZAR MILAGROS JAZMIN
CIVIL ENGINEERING UNDERGRADUATE STUDENT, UNIVERSIDAD PRIVADA DEL NORTE, FACULTY OF ENGINEERING, LIMA, PERÚ
EMAIL: n00337990@upn.pe, ORCCID ID: HTTPS://ORCID.ORG/0009-0002-7376-8929

CARMONA ARTEAGA ABEL
MASTER OF SCIENCE IN WATER RESOURCES, UNIVERSIDAD PRIVADA DEL NORTE, FACULTY OF ENGINEERING, LIMA, PERÚ
EMAIL: abel.carmona@upn.edu.pe, ORCID ID: 3HTTPS://ORCID.ORG/0000-0003-2895-9582

Abstract— This study aimed to design and analyse the performance of an innovative fluid energy dissipator model, comparing its behaviour in Autodesk CFD simulations with the experimental tests performed. The flow behaviour at different inlet velocities is examined to identify the ability of the dissipator to control the flow regime and minimize its energy under channel conditions, particularly under laminar and turbulent flows. The results revealed that, under various inlet conditions, the design maintained a tendency towards a stable flow in laminar and turbulent conditions, even in high velocity situations, with localized presences of turbulence in strategic areas. These areas, generated by negative pressures and vortices in the inner cavity of the dissipators, promoted energy dissipation along the structure and demonstrated an effective reduction of the exit velocity.
Keywords: Autodesk CFD, energy reduction, Hydraulic energy dissipators, speed reduction.

INTRODUCTION

Peru, due to its geographical location and rugged terrain, is highly susceptible to the occurrence of huaycos. These natural phenomena, also referred to as landslides or debris flows, are recurrent in the country, particularly in the highland and coastal regions. Seasonal rainfall and steep topography make these areas especially prone to significant hazards. Between 2003 and 2019, more than 2,000 huaycos were recorded in Peru, affecting thousands of people and causing substantial material and economic losses [1]. These landslides, composed of a mixture of water, rocks, and sediments, are triggered by intense rainfall and exacerbated by erosion and deforestation, which heighten the country's vulnerability to such disasters.

To mitigate the consequences of these events, energy dissipators are employed, whose primary function is to distribute the flow and reduce its energy. Energy dissipation can be achieved through various methods, depending on the type of structure to be built or already in place, as well as factors such as slope, dimensions, and the type of material in the discharge area (e.g., rock or sediment). These considerations are critical in the selection of an appropriate energy dissipator [2].

Energy dissipation plays a crucial role in ensuring that the flow enters downstream channels under normal and calm conditions. This is achieved by reducing the velocity of the flow, thereby preventing the scouring of hydraulic structures and erosion downstream. The phenomena involved in energy dissipation are inherently three-dimensional and require precise investigation and measurement through physical modeling [3].

However, an important criterion when conducting physical modeling is the significance of the structure being analyzed.

For complex structures whose failure could lead to severe consequences, the associated high costs of investment often render continued investigations unfeasible.

Between the 1950s and 1960s, computational methods, such as Computational Fluid Dynamics (CFD) software, were proposed as an alternative to reduce the costs associated with physical modeling. However, due to the lack of computational capacity at that time, significant progress in this field was limited [4].

Today, advancements in technology have enabled the modeling of these structures using CFD software. This allows for the simulation of both real and canonical flows, thereby reducing the time and costs associated with

experimentation. CFD simulations provide insights into the mechanical energy dissipation of the flow, the symmetry of water flow, as well as the distribution of velocity and pressure [4].

For this reason, the present study evaluated the behavior of water velocities and pressures through a two-dimensional simulation using CFD software. Additionally, a three-dimensional physical model was developed for greater accuracy, with the aim of comparing the water flow behavior between the simulation and experimental results.

I. RESEARCH OBJECTIVE

According to the problem posed, the objective is to design and analyze a system of energy dissipator structures using computational fluid dynamic (C.F.D.) software with the purpose of effectively reducing pressures and flow velocities, validating it through comparison with a physical model and obtain more accurate behavior in both simulations.

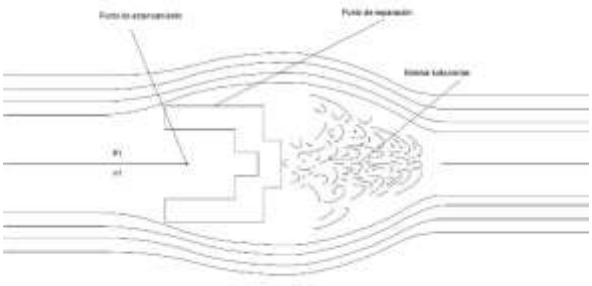

II. THEORETICAL FRAMEWORK

A. Autodesk CFD

Computational Fluid Dynamics (CFD) encompasses the knowledge and tools used to solve the mathematical models governing fluid dynamics phenomena through computational software. This approach allows for the prediction and manipulation of fluid behavior in any industrial process equipment. However, even when employing simplified equations and high-performance computers, only approximate solutions can be achieved [5].

B. Autodesk Inventor

Autodesk Inventor software offers a set of easy-to-use tools for 3D mechanical design, documentation, and product simulation. Digital prototyping with Inventor helps you design and validate your products before they are manufactured to deliver better results, reduce development costs, and get them to market faster using specialized digital modeling tools [6].

C. Hydraulic energy sink

Energy dissipators are hydraulic structures used to reduce excess kinetic energy of the flow, expressed in high speeds, which, when attempted to be reduced, produce high pressures and the appearance of hydraulic jumps and water impacts on the exposed material, thereby preventing downstream erosion [7].

D. SST K-Omega RC Model (Hellsten)

This model is based on the same k−ωk-\omegak−ω SST combination, providing high precision in the boundary layer and stability in regions far from the walls. It allows the effects of curvature and rotation to be captured more accurately, which is useful in applications where rotational forces and curved geometry significantly affect the turbulence structure [10].

E. Drag Force

The drag force must be counteracted by a propulsion force applied in the opposite direction in order to maintain or increase the speed of the vehicle. Because the production of propulsion force requires additional power, it is desirable to minimize the drag force [9].

$$C_d = \frac{2 \cdot F \cdot d}{\rho \cdot v^2 \cdot A} \quad (1)$$

Cd: drag coefficient
ρ: fluid density
v: velocity of the free flow of the fluid relative to the body.
A: characteristic area of the body

Fig. 1 Stagnation point, detachment and wake turbulence generated in the inverted horseshoe heatsink

Fig. 1 Stagnation point, detachment and wake turbulence generated in the inverted horseshoe heatsink

F. Vorticity

In general, most fluids that move from one point to another generate a phenomenon that is usually known as flow rotation. In this way, vorticity becomes the mathematical quantification of flow rotation; that exists within any fluid that is in motion; This expression is usually expressed vectorally [10].

G. Stagnation point

The stagnation point is defined as the place where the velocity within a flow field is equal to zero, this is due to the impact of the fluid with a surface or where the fluid will rest, in this way it can be concluded that it is also the place where there is the greatest pressure [10].

H. General energy equation

One of the fundamental laws of nature is the first law of thermodynamics, also known as the principle of conservation of energy, which provides a solid basis for studying the relationships between various forms of energy and their interactions. It states that energy cannot be created or destroyed during a process; it only changes forms [11].

$$\frac{v_1^2}{2g} + \frac{P_1}{\gamma} + z_1 = \frac{v_2^2}{2g} + \frac{P_2}{\gamma} + z_2 + h_T \quad (2)$$

P: pressure
V: flow speed
Z: height with respect to the origin
γ: specific weight of fluid
g: gravity

h_T: total losses

I. Reynolds number

Osborne Reynolds discovered that the flow regime depends primarily on the ratio of inertial forces to viscous forces in the fluid. Furthermore, the Reynolds number is a dimensionless quantity, which allows determining the behavior that occurs within a duct or around an object [12].

$$Re = \frac{D \cdot v \cdot \rho}{\mu} \quad (3)$$

$$D_P = \frac{4 \cdot a \cdot b}{2(a+b)} \quad (4)$$

Re: Reynolds number
D: Hydraulic Diameter (m)
V: Fluid velocity (m/s)
ρ: Fluid density (kg/m^3)
μ: fluid dynamic viscosity (Pa.s)

J. Laminar and turbulent flow

In laminar flow, the fluid moves in parallel layers without mixing between them, characterized by ordered and stable trajectories under conditions of low velocity and high viscosity. This flow regime is typical for values of the Reynolds number (Re) less than or equal to 500 in channels [13].

While turbulent flow is a type of movement in which the fluid presents irregular changes in speed and direction, with mixing between layers and the formation of eddies and vortices. This flow is common at high speeds and with low viscosity fluids, characterized by its chaotic and complex nature, which can reach Re values greater than 500 [14].

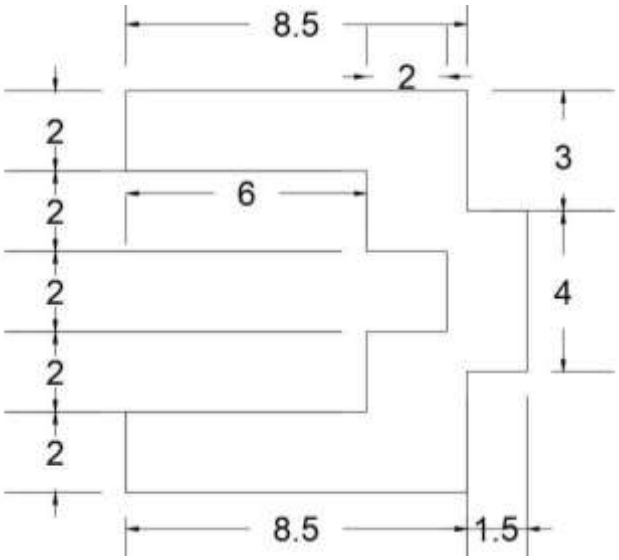

K. Navier - Stokes equation

The Navier-Stokes equation arises from applying Newton's second law, or law of force, to an element of mass subjected to the interactions of stress forces, in which pressure participates; and to body forces, among which are friction and gravity; together with the condition of conservation of mass, which due to the characteristic of the incompressibility of the fluid, becomes the absence of divergence; and where, in addition, the initial condition for the fluid velocity must be added [15].

$$\rho \frac{D_u}{D_t} = \left(-\frac{\partial P}{\partial x}\right) + (\rho \cdot g_x) + (\mu \cdot \nabla^2 \cdot u) \quad (5)$$

$$\rho \frac{D_v}{D_t} = \left(-\frac{\partial P}{\partial y}\right) + (\rho \cdot g_y) + (\mu \cdot \nabla^2 \cdot v) \quad (6)$$

$$\rho \frac{D_w}{D_t} = \left(-\frac{\partial P}{\partial z}\right) + (\rho \cdot g_z) + (\mu \cdot \nabla^2 \cdot w) \quad (7)$$

$$\nabla^2 = \frac{\partial^2}{\partial x^2} + \frac{\partial^2}{\partial y^2} + \frac{\partial^2}{\partial z^2} \quad (8)$$

METHOD

Next, we mention the design procedure in the Inventor software, the two-dimensional CFD simulation and finally the laboratory test carried out in the laminar flow machine with sources and sinks.

We started by creating the geometry of our heatsink. In our research, we wanted its shape to be symmetrical, with

a non-complex geometry and to be efficient for energy dissipation.
For this reason, the heatsink design chosen was an inverted horseshoe shape. This was modeled in the AutoCAD software, which was thought to have straight edges, for greater simplicity and to present a large space within its internal concavity for greater energy dissipation, which is why the dimensions were given to be 10 cm x 10 cm, and the prototype can be shown in Figure 2.

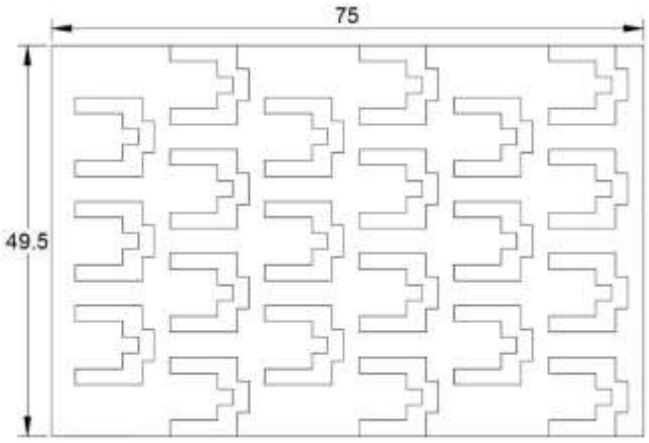

Fig. 2 Dimensions of the designed heatsink

After that, our design was captured in a rectangle simulating the laboratory table with its respective dimensions. Obtaining the following order, 3 columns of 3 rows and 3 columns of 4 rows within the water table, as shown in Figure 3. Having a spacing between rows and columns of 3.2 cm and 2 cm respectively.
Fig. 3 2D design of the heatsink and the test table with their respective dimensions

Following this, we imported our design made in AutoCAD into the Autodesk Inventor software. To do this, we open the program, select Start 2D Sketch, choose the XY plane, import and insert the Scale command to provide a scale of 10, since later in the Autodesk CFD program it is placed in the unit of millimeters (mm). Finally, we insert the Patch command to the surface through which the fluid will pass, this configuration helps us extrude a surface keeping it in 2D.
Once the design of the heatsink has been defined in 2D, we will carry out the 3D physical modeling to carry out the simulation in the laboratory using the laminar flow machine with sources and sinks. In our case, we make the molds based on a mixture of cement, plaster and water, giving them a height of 5 cm. and after drying, it was sanded to give it a finish without imperfections and to reduce the error in the experimental simulations.
Once the 21 molds are ready, we will proceed to place them on top of the testing table, as can be seen in Figure 4, to carry out the tests in laminar and turbulent flow. To do this, we open the water tap that is located at the back of the flow machine a little, so that the elevated tank fills and thus supplies water to the entire flow machine.

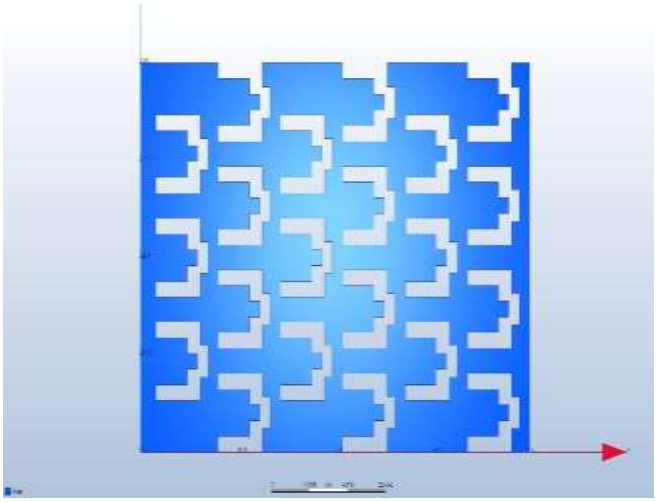

Fig. 4 Placing heatsinks on the test table
Then we proceed to open the other key located at the other end on the side of the flow machine. By opening the aforementioned tap, the entire glass table and the first container of the machine will begin to fill. In this way we will

obtain the flow rate and the Reynolds number.

Fig. 5 Procedure to find the Reynolds number in the laboratory

Figure 5 shows the steps required to find the Reynolds number, which will assign the type of flow in each simulation. Having now the complete heatsink design in the Autodesk Inventor software, we will export it to the Autodesk CFD program, as can be seen in Figure 6.

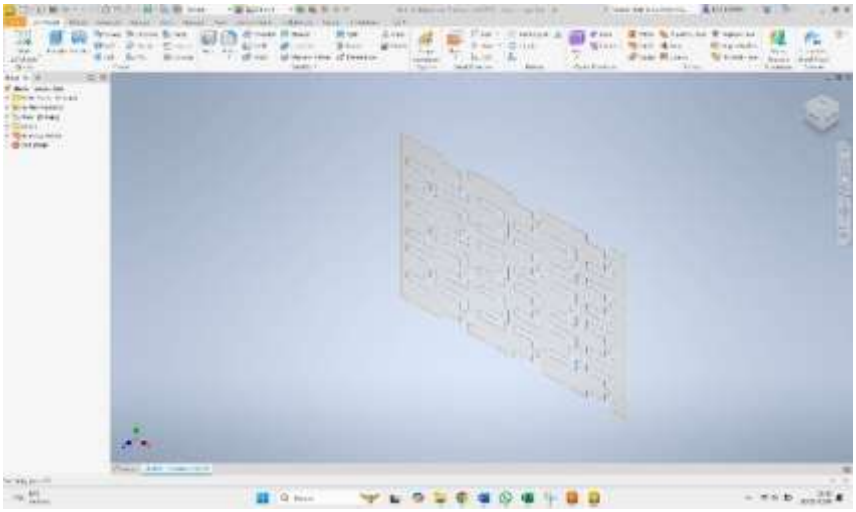

Fig. 6 Creating heatsinks in Autodesk Inventor

TPM Vol. 32, No. S6, 2025
ISSN: 1972-6325
https://www.tpmap.org/

Open Access

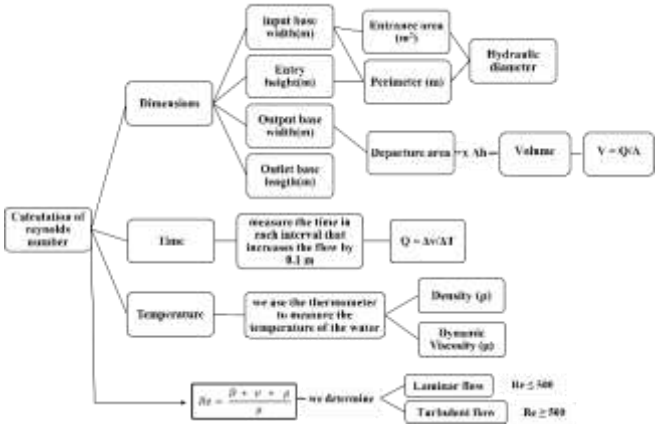

Fig. 7 Export of the design to Autodesk CFD.

The simulations carried out in the laboratory resulted in a laminar and turbulent flow, so we will begin by assigning the type of material "water", for Boundary Conditions we assign the inlet velocities by selecting the surface lines parallel to the Y axis. In the same way we place the inlet pressure and outlet pressure.

For the Mesh Size, we delimit a value of 0.5 mm which will capture more details and give a more precise result. For iterations a we assign a value of 1000.

We choose the solve option and we will enter the type of flow that we will simulate with respect to speeds, in our case it will be laminar and turbulent type.

Finally we click Solve and wait for the simulation to be carried out according to the data entered.

RESULTS

In this research, a comparison was carried out between the simulations carried out in Autodesk CFD and the experimental tests to study the cinematographic behavior of water. The results obtained will allow us to analyze the effectiveness of the energy dissipator in reducing erosion in channels. To do this, the Reynolds number will be calculated, providing a precise analysis of the flow regime to which our inverted horseshoe-shaped heatsink is subjected, this indicator being fundamental to determine the effectiveness of the system in specific hydraulic conditions and its ability to minimize the erosive effects. Therefore, for the analysis of the behavior of laminar or turbulent flow, simulations in the Autodesk CFD program help to understand the behavior of our profiles under certain flows, comparing it with real simulations tested in the laboratory.

It is important to highlight that, for the determination of the Reynolds number, there are some constant data that were maintained in the 2 simulations carried out, which are the temperature, density of the fluid (water) and dynamic viscosity.

TABLE I CONSTANT FLOW DATA TO DETERMINE THE REYNOLDS

Temperature	Density	Dynamic Viscosity
(C°)	(Kg/m3)	(Pa.s)
19.4	998.68	0.0010356

For the first analysis, the entry velocity of the water flow was established, which was calculated at 0.01723 m/s. This value was obtained by measuring the temporal variations of the flow in a range of 10 intervals, considering that, under ideal conditions, the inlet flow is equivalent to the outlet flow. Using this premise, and with the known dimensions of the outlet container (9.3 cm base and 60 cm length), a constant volume is calculated. Each interval is set to 1 cm, allowing for detailed and accurate measurement of muzzle velocity. Subsequently, the outlet flow was divided by the inlet area to calculate the inlet velocity. Furthermore, it is important to highlight that a constant water height of 0.5 cm was maintained at the inlet throughout the experiment, which guarantees a stable condition for repeated measurements. With the data obtained, it is possible to calculate the Reynolds number, which provides a clear description of the flow regime, whether laminar or turbulent. This parameter is essential to characterize the behavior of the fluid in the system and evaluate the effectiveness of our energy dissipators.

TABLE II RECORD OF TIME VARIATIONS FOR LAMINAR FLOW

H accumulated	Time (1)	Time (2)	Time (3)	Time (4)	Time average
0.01	13.74	13.69	13.65	13.58	13.67
0.02	14.25	14.35	14.27	14.23	14.28
0.03	14.06	14.04	14.02	14.01	14.03

0.04	12.31	12.25	12.34	12.29	12.3
0.05	14.29	14.34	14.25	14.25	14.28
0.06	13.28	13.27	13.4	13.44	13.35
0.07	12.41	12.42	12.33	12.27	12.36
0.08	10.77	10.78	10.8	10.83	10.8
0.09	13.2	13.12	13.22	13.18	13.18
0.1	13.37	13.57	13.47	13.5	13.48
Total time average					**13.17**

TABLE III CALCULATION OF AVERAGE INLET VELOCITY FOR LAMINAR FLOW

Δh	**Δ Volume**	**Q exit**	**Entry speed**
(m)	**(m3)**	**(m3/s)**	**(m/s)**
0.01	0.000558	$4.08342*10^{-5}$	0.01650
0.01	0.000558	$3.90893*10^{-5}$	0.01579
0.01	0.000558	$3.97648*10^{-5}$	0.01607
0.01	0.000558	$4.53751*10^{-5}$	0.01833
0.01	0.000558	$3.90688*10^{-5}$	0.01579
0.01	0.000558	$4.18056*10^{-5}$	0.01689
0.01	0.000558	$4.51548*10^{-5}$	0.01824
0.01	0.000558	$5.16906*10^{-5}$	0.02089
0.01	0.000558	$4.23369*10^{-5}$	0.01711
0.01	0.000558	$4.14023*10^{-5}$	0.01673
Average total speed			**0.01723**

TABLE IV CALCULATION OF THE REYNOLDS NUMBER FOR LAMINAR FLOW

Water density	**Entry speed**	**Hydraulic diameter**	**Dynamic viscosity**	**Result**
(Kg/m3)	**(m/s)**	**(m)**	**(Pa.s)**	**-**
998.68	0.01723	0.01960	0.0010356	325.80

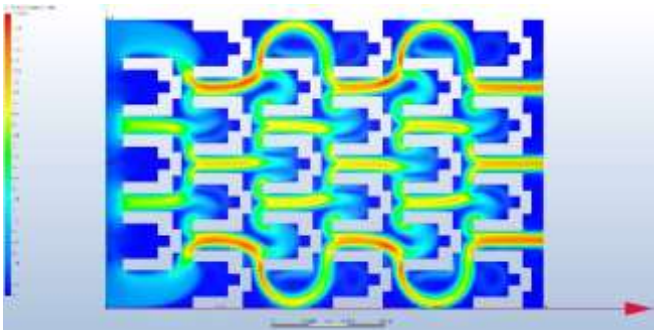

Fig. 8 CFD simulation of our heatsink with a speed of 0.01723 m/s in a laminar flow.

Figure 8 illustrates a gradual decrease in flow velocity in the areas of greatest aperture, specifically in rows 1, 3 and 5, due to the inversely proportional relationship between the length of these areas and the flow velocity. This effect contrasts with the notable increase in velocity observed in the areas located between the heatsinks of rows 2, 4 and 6. It should be noted that, upon reaching the centroid of the heatsinks, a marked reduction in flow speed is evident, attributable to to the presence of negative pressures generated in these regions.

This phenomenon is the result of the interaction of opposite flows that are found at these points; When the water flow enters in the direction of the positive This reversal creates zones of minimum velocity, thus achieving efficient dissipation of water energy in the system.

Figure 9 shows the flow of water moving through our heatsink structure, where areas of high turbulence and vortices form in the areas of greatest amplitude between the heatsinks. As the flow progresses, the trajectories of the water particles show curves and eddies around the edges of the sinks, suggesting that the structure is generating abrupt changes in flow direction. This, as in the simulation in the Autodesk CFD program, is especially notable in the center of the heatsinks, where a concentration of dark areas is observed, which suggests the presence of negative pressures generated by the collision of flows in opposite directions. These low velocity, high turbulence zones function to dissipate the water's energy in a controlled manner.

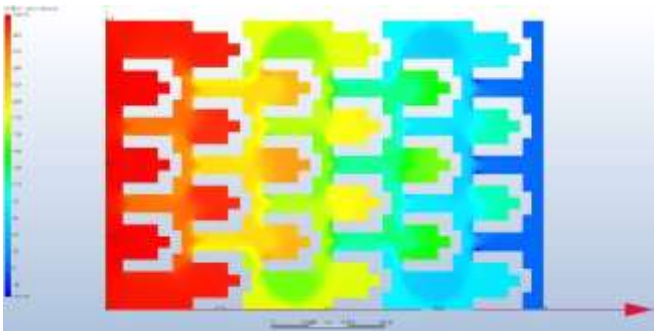

Fig. 9 Simulation on the test table with a speed of 0.01723 m/s

By comparing this image with the simulation results in the CFD software, it is confirmed how the heatsink manages to reduce inlet velocities by increasing low pressure zones, as seen in Figure 10. This visual analysis validates the coherence between the digital model and the physical one, showing that both manage to reproduce the expected flow characteristics and the effect of energy dissipation through negative pressures and localized turbulence.

Fig. 10 Pressure flow in the laminar simulation.

In the second analysis, we sought to determine the behavior of our heatsinks in the face of a turbulent flow by increasing the inlet velocity, since the characteristics and/or conditions of the fluid in this case are more similar to the problem of our research, which is the huayco Therefore, the determination of the inlet velocity was obtained through the controlled expansion of the water system in the laboratory.

Using the information provided above, we calculate the inlet velocity and Reynolds number.

TABLE V RECORD OF TIME VARIATIONS FOR TURBULENT FLOW

H accumulated	**Time (1)**	**Time (2)**	**Time (3)**	**Time (4)**	**Time average**
0.01	3.15	3.16	3.17	3.13	3.15
0.02	2.43	2.43	2.41	2.44	2.43
0.03	2.47	2.5	2.45	2.43	2.46
0.04	2.29	2.25	2.23	2.22	2.25
0.05	2.11	2.16	2.1	2.12	2.12
0.06	2.18	2.13	2.14	2.15	2.15
0.07	2.21	2.2	2.18	2.19	2.2
0.08	2.41	2.45	2.39	2.37	2.41
0.09	2.08	2.1	2.05	2.07	2.08
0.1	2	1.93	2.1	2	2
Total time average					**2.32**

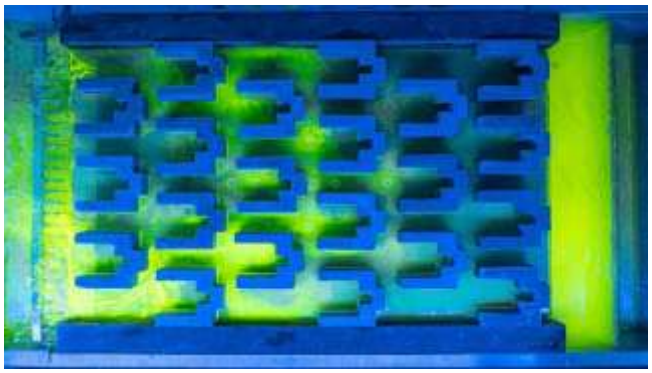

TABLE VI CALCULATION OF AVERAGE INLET VELOCITY FOR TURBULENT FLOW

Δh	**Δ Volume**	**Q exit**	**Entry speed**
(m)	**(m3)**	**(m3/s)**	**(m/s)**
0.01	0.000558	$1.77002*10^{-4}$	0.01788
0.01	0.000558	$2.29866*10^{-4}$	0.02322
0.01	0.000558	$2.26599*10^{-4}$	0.02889
0.01	0.000558	$2.48276*10^{-4}$	0.02508
0.01	0.000558	$2.62898*10^{-4}$	0.02656
0.01	0.000558	$2.59535*10^{-4}$	0.02622
0.01	0.000558	$2.54214*10^{-4}$	0.02568
0.01	0.000558	$2.32017*10^{-4}$	0.02344
0.01	0.000558	$2.68916*10^{-4}$	0.02716
0.01	0.000558	$2.77958*10^{-4}$	0.02808
Average total speed			**0.02462**

TABLE VII CALCULATION OF THE REYNOLDS NUMBER FOR TURBULENT FLOW

Water density	**Entry speed**	**Hydraulic diameter**	**Dynamic viscosity**	**Result**
(Kg/m3)	**(m/s)**	**(m)**	**(Pa.s)**	**-**
998.68	0.02462	0.07402	0.0010356	1757.30

As can be seen in table 5, the time intervals range between 2 – 3 seconds, which ensures that the water level is increasing rapidly due to the high speed it presents. Furthermore, as seen in Table 7, the Reynolds number obtained in this simulation was clearly turbulent, this being mentioned previously due to the increase in the inlet velocity.

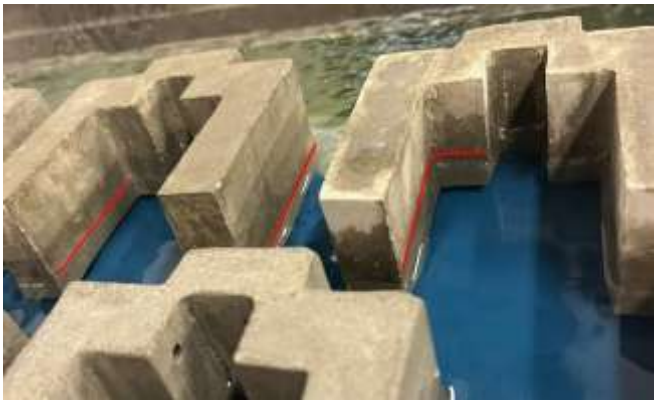

Fig. 11 Variation of water level

A relevant aspect in this simulation was the variation of flow heights throughout the dissipator system. From the water inlet to the second row of sinks, both inside and between them, an average height of 2 cm was recorded. In the intermediate section, which spans from the third to the fifth row, the water level decreased to 1.8 cm. Finally, in the last section, more complex height variations were observed: at the centroid of each heatsink, the level remained at 1.8 cm, while, in the spaces between heatsinks, the height dropped to 1.5 cm, as shown in Figure 11. The variation

in flow heights is directly related to the friction losses described in the energy equation. This phenomenon occurs because the fluid enters with an initial energy, which progressively decreases as it passes through the successive rows of the heatsinks. These energy losses are due to the friction generated by the roughness of the heatsinks and the interaction of the fluid with the solid surfaces, being closely linked to the dynamic viscosity of the fluid.
This interaction induces the formation of a boundary layer, where velocity gradients develop that generate short stresses. These efforts, resulting from the viscosity of the fluid, transform part of the kinetic energy of the flow into thermal energy, contributing to the progressive dissipation of energy throughout the system. This process, in turn, causes a gradual reduction in the water level in the canal.

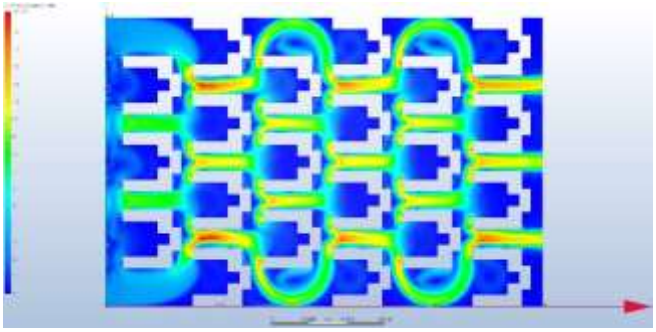

Fig.12 Simulation on the test table with a speed of 0.02462 m/s.
Fig. 13 CFD simulation of our heatsink with a speed of 0.02462 m/s in a turbulent flow – SST equation k – omega RC (Hellsten)
In this analysis, similar to the previous test, it was observed that the water flow showed a predominantly turbulent behavior. This prompted 10 additional simulations to be performed in Autodesk CFD, evaluating a series of turbulent flow modeling equations. Among these, the equation that presented the greatest similarity with the behavior observed in the test was that of SST k-omega RC (Hellsten). This model allowed us to identify specific zones of turbulence located not only inside the heatsinks in rows 1 to 3, but also along the edges of each heatsink. This phenomenon is attributed to the increase in the inlet velocity achieved in this test, which intensifies the flow interactions along the elements. In addition, the presence of areas with more abundant negative pressures was noted in the internal cavities of the heatsinks located at the ends of the system, as shown in Figure 14. These areas of negative pressure generate longer lasting wakes, reinforcing the effectiveness of the design to induce low flow conditions and energy dissipation in strategic regions of the system. This result underscores the ability of the SST k-omega RC (Hellsten) model to accurately capture the turbulent flow dynamics and dissipative effects of our design under high velocity conditions.

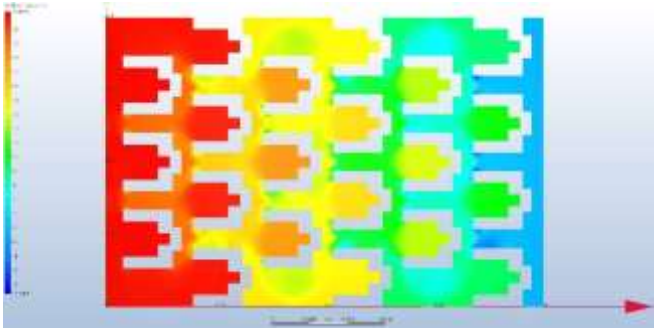

Fig. 14. Pressure flow in turbulent simulation with speed of 0.02462m/s

Fig. 15 Generation of longer duration contrails due to negative pressure

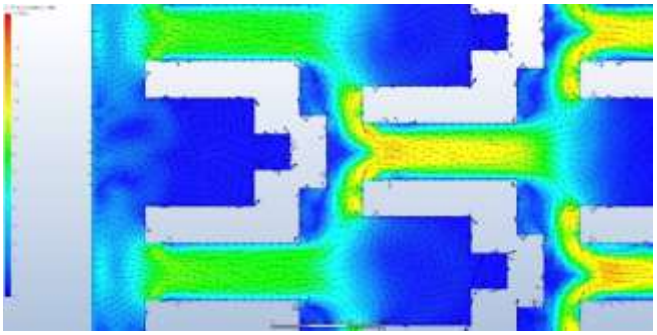

Fig. 16 Generation of zones with negative pressures and water flow behavior in Autodesk CFD

This behavior is seen more clearly in Figures 15 and 16, where it is observed that the vector direction of the flow is initially oriented on the positive x axis. However, when interacting with the internal wall of the heatsink, the flow changes its direction towards the negative x-axis, generating characteristic phenomena such as the Von Kármán effect and the formation of vorticities. These interactions lead to a significant reduction in fluid velocity, which in turn causes the formation of wakes and negative pressure regions on the surfaces of the heatsinks.
This analysis reveals a direct correlation between the results obtained in the experimental tests carried out in the laboratory and the numerical simulations developed with the Autodesk CFD software. This correspondence validates the effectiveness of the heatsink design in attenuating the kinetic energy of the flow, highlighting its ability to control the hydraulic behavior under specific operating conditions. These observations reinforce the reliability of the designed system and its applicability in the efficient management of hydraulic flows.
According to the variations in height and Reynolds number calculated in each simulation, we make the following table.

TABLE VIII SUMMARY OF RESULTS

Simulations	**Δ of height**	**Δ Entry speed**	**Reynolds Number**
First	0.5 cm	0.01723 m/s	325.80
Second	2 cm	0.02462 m/s	1757.30

As seen in Table 8, in the simulations carried out, the increase in the inlet velocity has produced a significant increase in the Reynolds number compared to the first and second simulation, however, due to the geometry and distribution of our heatsink in inverted horseshoe shape, allows the flow to remain in a stable regime in all simulations. This behavior constitutes a particular case that reflects the efficiency of the energy dissipator design. As the inlet velocity increases, the system exhibits a pond-like effect, in which the increase in velocity generates fluid retention which, in turn, increases the height of the water in contact with the heatsinks.
This design feature allows that, although specific areas of turbulence are generated, especially at strategic points, the internal structure of the heatsink continues to effectively dissipate the energy of the flow. The heatsink geometry is optimized to minimize output velocity, achieving significant energy attenuation through controlled dissipation in its internal cavities. This retention and dissipation behavior demonstrates the effectiveness of the design in reducing flow intensity, contributing to precise control of the hydraulic regime in the channel.

CONCLUSIONS

Based on the comprehensive work conducted in this research, it is concluded that the design of our inverted horseshoe-shaped energy dissipator for flows is remarkably effective and exhibits uniquely efficient performance at both low and high velocities. The results obtained, both from CFD software simulations and physical-experimental tests, reveal extensive zones of negative pressure and abrupt dissipation of turbulent flows in strategic areas, regardless of the inlet velocity. This is supported by Reynolds number calculations and the water's behavior under laminar and turbulent flow conditions, suggesting that the design is capable of maintaining a predominantly stable flow throughout the channel.
Furthermore, the design has demonstrated a high energy dissipation capacity through the formation of zones exhibiting the Von Kármán effect (vorticity) and areas of reduced flow, creating so-called "dead zones" where fluid velocity decreases significantly. This effect not only facilitates the transformation of a potentially turbulent flow into a more stable and laminar flow but also ensures a controlled and reduced outlet velocity compared to the inlet velocity. As the flow progresses through the dissipators, a gradual reduction in water level occurs, contributing to the system's stability without compromising the outlet velocity or the functionality of the dissipator.
The specific geometry of our design enables more precise control of flow dynamics, resulting in a prolonged and efficient energy dissipation process. Additionally, under flow conditions containing sedimentary materials, this

design may provide an added advantage by promoting sediment retention in wake zones created by negative pressures at the dissipators' centers of mass. This feature could prove particularly beneficial in natural events such as debris flows (huaycos). This characteristic distinguishes our dissipator from conventional and more complex geometries, as it not only effectively reduces the kinetic energy of water but also facilitates controlled sediment deposition in targeted areas. Over time, this would significantly reduce societal repair costs associated with debris flow damage.

Finally, the proposed inverted horseshoe-shaped energy dissipator not only fulfills the objectives of this research by providing an effective energy dissipation system but also offers significant practical advantages for sediment flow control and erosion mitigation in channels. The dissipator's ability to transform potentially turbulent flows into stable flows, along with its efficiency under variable water velocity and volume conditions, positions this design as a robust and innovative solution in flow management and erosion control engineering.

REFERENCES

[1] Instituto Nacional de Defensa Civil (INDECI). (2020). Información estadística de emergencias y daños, periodo 2003 al 2019.
https://portal.indeci.gob.pe/wp-content/uploads/2021/02/CAPITULO-III-Estad%C3%ADstica-Series-2003-2019.pdf

[2] 2. Preguntegui, G. (2023). Preservación de los canales de drenaje mediante el empleo de disipadores de energía: el caso del canal en el distrito de Carmen Alto en Huamanga. Tesis para optar el título profesional de Ingeniero Civil, Universidad Continental Repositorio institucional de la Universidad Continental. https://repositorio.continental.edu.pe/handle/20.500.12394/13430

[3] Paredes, R. (2014). Investigación de la disipación de energía del segundo aliviadero de excedencia-Presa Sabana Yegua. Tesis de pregrado no publicado en Ingeniería Civil, Universidad de Piura. Repositorio institucional de la Universidad de Piura.
https://gestionrepo.udep.edu.pe/items/8d7f54b1-4b27-417a-8d59-6161c8cc0e4d

[4] Fernández, J. (2012). Técnicas numéricas en ingeniería de fluidos: Introducción a la dinámica de fluidos computacional (CFD) por el método de volúmenes finitos.Editorial Reverté. S.A. https://books.google.es/books?hl=es&lr=&id=x9zeDwAAQBAJ&oi=fnd&pg=PR7&dq=Introducci%C3%B3n+a+la+Din%C3%A1mica+de+Fluidos+Computacional+(CFD)+como+herramienta+para+el+an%C3%A1lisis+de+flujos+fluidodin%C3%A1micos.&ots=DpL_DUbu5I&sig=-KRfJvCeVpuYMSR2gkRh0cgzU_4#v=onepage&q&f=false

[5] Zamora, M. (2016). Simulación numérica de la inyección de gas en columnas de flujo oscilatorio. Tesis para optar el título profesional de Ingeniero Industrial, Universidad Politécnica de Cartagena. Repositorio institucional de la Universidad Politécnica de Cartagena.
https://repositorio.upct.es/entities/publication/9aad1be0-e784-4fb0-a25b-93bd16b18b73

[6] Valdebenito, P. (2018). Análisis estático estructural de un dispositivo de aprovechamiento de energía mareomotriz a emplear en el canal de Chacao. Informe de Habilitación Profesional presentado en conformidad a los requisitos para optar al Título de Ingeniero Civil Mecánico, Universidad del Bío-Bío. Repositorio institucional de la Universidad del Bío-Bío.
http://repobib.ubiobio.cl/jspui/handle/123456789/3399?mode=full&submit_simple=Mostrar+el+registro+Dublin+Core+completo+del+%C3%ADtem+

[7] Ayala, L. et al. (2019). Evaluación de la eficiencia en disipación de energía en estructuras hidráulicas construidas con gaviones y material reciclado (neumático usado) mediante modelamiento físico a escala reducida. Redalyc. https://www.redalyc.org/journal/5537/553768131014/

[8] Jaramillo, J., Cárdenas H. (2015). Numero de Reynolds. Proyecto de grado. Repositorio institucional de la Corporación Universitaria Minuto De Dios sede regional Girardot.
https://repository.uniminuto.edu/server/api/core/bitstreams/ae6f9282-d8d4-4081-8d79-e421c12d01ec/content

[9] Mott, R., & Untener, J. (2015). Número de reynolds, flujo laminar, flujo turbulento y pérdidas de energía por fricción. En Mecánica de Fluidos (7.aed.).
https://www.academia.edu/43741728/Mecanica_de_Fluidos_7a_ed_Mott

[10] Tibabisco, C. (2018). Análisis de la transferencia de calor por impacto a través del número de nusselt en el punto de estancamiento sobre una placa plana. Proyecto de grado, Universidad Libre. Repositorio institucional de la Universidad Libre. https://repository.unilibre.edu.co/handle/10901/11559

[11] Cengel, A., Boles, M. (2012). Temodinámica. (7a ed.). McGraw-Hill.
https://www.academia.edu/39821820/Termodin%C3%A1mica_Cengel_and_Boles_7ma_edici%C3%B3n

[12] Çengel, A., Cimbala, M. (2006). Mecánica de fluidos: Fundamentos y aplicaciones (1a ed.). McGraw-Hill.
https://www.academia.edu/25669790/Mecanica_de_Fluidos_Fundamentos_y_Aplicaciones_Yunus_Cengel_y_John_Cimbala_Primera_Edicion

[13] Fox, R. W., & McDonald, A. T. (1995). Introducción a la mecánica de fluidos (4a ed.). Wiley.
https://www.academia.edu/34612346/INTRODUCCI%C3%93N_A_LA_MEC%C3%81NICA_DE_FLUIDOS